A&A, 684, L3 (2024)
https://doi.org/10.1051/0004-6361/202449639

Astronomy & Astrophysics

LETTER TO THE EDITOR

Tidal frequency dependence of the Saturnian k_2 Love number

V. Lainey[1], J. W. Dewberry[2], J. Fuller[3], N. Cooper[4], N. Rambaux[1], and Q. Zhang[5]

[1] IMCCE, Observatoire de Paris, PSL Research University, CNRS, Sorbonne Université, Univ. Lille, France
e-mail: valery.lainey@obspm.fr
[2] Canadian Institute for Theoretical Astrophysics, 60 St. George Street, Toronto, ON M5S 3H8, Canada
[3] TAPIR, Mailcode 350-17, California Institute of Technology, Pasadena, CA 91125, USA
[4] Department of Physics & Astronomy, Queen Mary University of London, Mile End Rd, London E1 4NS, UK
[5] Department of Computer Science, Jinan University, Guangzhou 510632, PR China

Received 16 February 2024 / Accepted 18 March 2024

ABSTRACT

Context. Love numbers describe the fluid and elastic response of a body to the tidal force of another massive object. By quantifying these numbers, we can more accurately model the interiors of the celestial objects concerned.
Aims. We determine Saturn's degree-2 Love number, k_2, at four different tidal forcing frequencies.
Methods. To do this, we used astrometric data from the *Cassini* spacecraft and a dynamical model of the orbits of Saturn's moons.
Results. The values obtained for k_2 are 0.384 ± 0.015, 0.370 ± 0.023, 0.388 ± 0.006, and 0.376 ± 0.007 (1σ error bar) for the tidal frequencies of Janus–Epimetheus, Mimas, Tethys, and Dione.
Conclusions. We show that these values are compatible with a constant Love number formulation. In addition, we compared the observed values with models of dynamical tides excited in Saturn's interior, also finding a good agreement. Future increases in the measurement precision of Love numbers will provide new constraints on the internal structure of Saturn.

Key words. astrometry – celestial mechanics – planets and satellites: dynamical evolution and stability – planets and satellites: fundamental parameters – planets and satellites: gaseous planets – planets and satellites: interiors

1. Introduction

Among the most surprising results obtained with the *Cassini* probe concerning the orbital dynamics of Saturn's moons was the quantification of tidal effects on Saturn. Using thousands of astrometric data points from the *Cassini* Imaging Science Subsystem (ISS) Narrow Angle Camera (NAC) images (Porco et al. 2004), Lainey et al. (2012) were able to measure the rapid orbital expansion of the moons. This is characterized by the tidal ratio k_2/Q, where k_2 is the degree-2 Love number and Q is the quality factor characterizing the dissipation of tidal energy in the planet. Using the motion of the four co-orbital moons of Tethys and Dione, Lainey et al. (2017) were able to independently quantify the two parameters, k_2 and Q. In a later work, Lainey et al. (2020) even managed to quantify the quality factor Q at six different frequencies, corresponding to the tidal frequencies associated with Mimas, Enceladus, Tethys, Dione, Rhea, and Titan.

In the present work, we investigated whether it is also possible to quantify Saturn's k_2 Love number at different tidal frequencies. Using all the astrometric data currently available, we show that it can be quantified at four tidal frequencies associated with the action of the moons Janus and Epimetheus (being on a horseshoe orbit, both moons share the same tidal frequency), Mimas, Tethys, and Dione. We then compared the results obtained with the values predicted by modelling the dynamical tidal response of the planet, including its fundamental and gravito-inertial modes and inertial waves.

In Sect. 2 we present the dynamical modeling used, as well as the fitting of the orbital model to astrometric data from the *Cassini* probe. In Sect. 3 we briefly present how Saturn's interior was modelled and compare the results obtained from astrometry with our model.

2. Orbital fit

We carried out orbital dynamical modelling and fitting to the observations in a similar way as Lainey et al. (2023, 2024), with the additional improvement of solving for an independent k_2 for the frequency of each tide-raising moon. For convenience, we review our method and the relevant equations below, and refer the reader to Lainey et al. (2023, 2024) for further details.

2.1. Dynamical modelling

Using the NOE (Numerical Orbit and Ephemerides) gravitational N-body code (Lainey et al. 2007), we fitted the full equations of motion (see Eq. (1)) to the available astrometric observations (see Sect. 2.2), solving for the initial positions and velocities of: the eight main moons; the four co-orbitals Telesto, Calypso, Helen, and Polydeuces; the five inner moons Atlas, Prometheus, Pandora, Janus, and Epimetheus; and the small moons Methone, Anthe, and Pallene. In addition, global parameters, such as the masses, the C_{np} and S_{np} gravity coefficients, and the Saturnian polar orientation, were simultaneously solved for. Following Lainey et al. (2023), the physical librations of Prometheus, Pandora, Janus, and Epimetheus were also considered. Lastly, the Saturnian Love number associated with each tide-raising moon was solved for, together with a supposedly constant Saturnian Love number, k_3.

Our model included (i) gravitational interactions up to degree 2 in the expansion of the gravitational potential of the satellites (Table 2 from Lainey et al. 2019) and degree 10 for Saturn (Iess et al. 2019); (ii) gravitational perturbations between all moons; (iii) the solar perturbation (where the masses of the inner planets and the Moon were incorporated into the solar mass) and the Jupiter perturbation based on the DE430 ephemeris; (iv) the precession of Saturn; (v) tidal effects based on the Love numbers k_2 and k_3, neglecting dissipation; and (vi) relativistic corrections.

Following Lainey et al. (2007), the equation of motion for a satellite P_i can be expressed as

$$\begin{aligned}\ddot{\boldsymbol{r}}_i = & -G(m_0+m_i)\left(\frac{\boldsymbol{r}_i}{r_i^3} - \boldsymbol{\nabla}_i V_{\bar{i}\hat{0}} + \boldsymbol{\nabla}_0 V_{\bar{0}\hat{i}}\right)\\ & + \sum\nolimits_{j=1,j\neq i}^{N} Gm_j\left(\frac{\boldsymbol{r}_j-\boldsymbol{r}_i}{r_{ij}^3} - \frac{\boldsymbol{r}_j}{r_j^3} + \boldsymbol{\nabla}_j V_{\bar{j}\hat{0}} - \boldsymbol{\nabla}_0 V_{\bar{0}\hat{j}} - \boldsymbol{\nabla}_j V_{\bar{j}\hat{i}} + \boldsymbol{\nabla}_i V_{\bar{i}\hat{j}}\right)\\ & + \frac{(m_0+m_i)}{m_i m_0}\boldsymbol{F}^T_{\bar{i}\hat{0}} + \sum\nolimits_{j=1,j\neq i}^{N}\left(-\frac{\boldsymbol{F}^T_{\bar{j}\hat{0}}}{m_0} + \frac{\boldsymbol{F}^T_{ij}}{m_i}\right) + GR, \end{aligned} \tag{1}$$

where $\boldsymbol{r}_i$ and $\boldsymbol{r}_j$ are the position vectors of satellite P_i and a perturbing body, P_j (another satellite, the Sun, or a planet) with mass m_j, respectively, the subscript 0 denotes Saturn, and $V_{\bar{k}\hat{l}}$ is associated with the gravity field of body P_l at the position of body P_k (including planetary oblateness). In particular, we have

$$V_{\bar{k}\hat{l}} = \sum_{n=1}^{\infty}\frac{R^n}{r^{n+1}}\sum_{p=0}^{n} P_n^p(\sin\phi)[C_{np}\cos p\lambda + S_{np}\sin p\lambda], \tag{2}$$

where R, C_{np}, and S_{np} are the radius and gravity field coefficients of the oblate body, P_l, while r, ϕ, and λ are the spherical coordinates of the disturbed object, P_k. Moreover, GR are corrections due to general relativity (Newhall et al. 1983). The $\boldsymbol{F}^T_{\bar{l}\hat{0}}$ is the force on P_l from the tides it raises on its primary body, and $\boldsymbol{F}^T_{ij}$ is the effect of tides raised by one moon on Saturn acting on another moon. In the absence of tidal dissipation, these last two forces are given by Lainey et al. (2007, 2017):

$$\boldsymbol{F}^T_{\bar{l}\hat{0}} = -\frac{3k_2 G m_l^2 R^5 \boldsymbol{r}_l}{r_l^8}, \tag{3}$$

$$\boldsymbol{F}^T_{ij} = \frac{3k_2 G m_j m_i R^5}{2r_i^5 r_j^5}\left[-\frac{5(\boldsymbol{r}_i\cdot\boldsymbol{r}_j)^2\boldsymbol{r}_i}{r_i^2} + r_j^2\boldsymbol{r}_i + 2(\boldsymbol{r}_i\cdot\boldsymbol{r}_j)\boldsymbol{r}_j\right]. \tag{4}$$

Here, the k_2 Love number is defined as

$$k_{np} = \frac{\delta\Phi_{np}}{U_{np}}, \tag{5}$$

where $\delta\Phi_{np}$ and U_{np} are coefficients associated with the angular dependence n, p in the perturbed and perturbing gravitational potentials. We assumed $k_2 = k_{20} = k_{21} = k_{22}$. A similar equation can be obtained with the third-order Love number, k_3:

$$\begin{aligned}\boldsymbol{F}^{T_{k_3}}_{ij} = & \frac{Gm_j m_i k_3 R^7}{2r_i^7 r_j^7}\left\{5(\boldsymbol{r}_i\cdot\boldsymbol{r}_j)\left[3r_j^2 - 7\frac{(\boldsymbol{r}_i\cdot\boldsymbol{r}_j)^2}{r_i^2}\right]\boldsymbol{r}_i\right.\\ & \left. +3[5(\boldsymbol{r}_i\cdot\boldsymbol{r}_j)^2 - r_i^2 r_j^2]\boldsymbol{r}_j\right\}. \end{aligned} \tag{6}$$

The physical libration of the moon P_i arises implicitly in the expression of $\boldsymbol{\nabla}_0 V_{\bar{0}\hat{i}}$ and $\boldsymbol{\nabla}_j V_{\bar{j}\hat{i}}$ in Eq. (1). For more details, the reader can refer to Eqs. (22) and (23) in Lainey et al. (2019).

Our fitting process involved solving the variational equations for an unspecified parameter, c_l, of the model to be fitted (e.g. $\boldsymbol{r}(t_0), \mathrm{d}\boldsymbol{r}/\mathrm{d}t(t_0), Q\ldots$; see Lainey 2016 for more details):

$$\frac{\partial}{\partial c_l}\left(\frac{d^2\boldsymbol{r}_i}{\mathrm{d}t^2}\right) = \frac{1}{m_i}\left[\sum_j\left(\frac{\partial \boldsymbol{F}_i}{\partial \boldsymbol{r}_j}\frac{\partial \boldsymbol{r}_j}{\partial c_l} + \frac{\partial \boldsymbol{F}_i}{\partial \dot{\boldsymbol{r}}_j}\frac{\partial \dot{\boldsymbol{r}}_j}{\partial c_l}\right) + \frac{\partial \boldsymbol{F}_i}{\partial c_l}\right]. \tag{7}$$

In this expression, $\boldsymbol{F}_i$ is the right-hand side of Eq. (1) multiplied by m_i. The partial derivatives of the solutions with respect to the initial positions and velocities of the satellites and the dynamical parameters were then computed via the simultaneous numerical solution of Eqs. (1) and (7), in a Saturn-centred frame with inertial axes based on the International Celestial Reference Frame.

To test the reliability of our fit, we considered extra perturbations. Among other effects, we considered the influence of Mimas's extended gravity field, the Saturnian nutations from the SAT427 SPICE kernel (Acton 1996), the Saturnian polar orientation determined by French et al. (2017), and the influence of using different *Cassini* orbit kernels. All these perturbations were found to be negligible within the uncertainty of our measurements.

In summary, all our simulations involved simultaneously solving for the initial state vectors and masses of the moons, the mass and gravity field of Saturn, including zonal harmonics up to order 10, the orientation and precession of Saturn, and the physical librations for Prometheus, Pandora, Janus, and Epimetheus. No constraints were introduced in the fit, except for Saturn's gravity field at the value estimated by Iess et al. (2019) assuming their published 1σ uncertainty. Last, we included the uncertainty on the tidal frequency dependence of the Saturnian Q parameter in the error bar of our measurements.

2.2. Fitting the data

We used all astrometric data available for the moons (Tajeddine et al. 2013, 2015; Cooper et al. 2014, 2018; Zhang et al. 2021; Lainey et al. 2023, 2024). Our astrometric residuals are given in Tables 1–3. To test the frequency sensitivity of the tidal frequency k_2 Love number, we used a two-step method. In the first step we solved for a constant k_2 and k_3 and obtained $k_2 = 0.384 \pm 0.004$ and $k_3 = 0.005 \pm 0.111$ (1σ error bar). In the second step, we solved for the k_2 at all of the moons' frequencies. Only four tidal frequencies could be fairly well constrained: the tides associated with Janus and Epimetheus, Mimas, Tethys, and Dione. In this second approach, we eventually used the constant k_3 and k_2 solution from the first approach for the other tidal frequencies.

From our second approach (using a non-constant k_2 Love number), we find that the Love number values obtained for the Janus–Epimetheus, Tethys, and Dione frequencies were obtained from cross tidal–tidal effects acting on the co-orbital moons. In other words, the tidal bulge of Saturn raised by one moon was measured through its effect on co-orbital moons in the exact same manner as described in Lainey et al. (2017). On the other hand, the signal at Mimas's tidal frequency was determined thanks to its resonance with Pandora. Our measurements for the Saturnian k_2 Love numbers are 0.384 ± 0.015, 0.370 ± 0.023, 0.388 ± 0.006, and 0.376 ± 0.007 at the Janus–Epimetheus, Mimas, Tethys, and Dione tidal frequencies, respectively.

3. Love number calculations

To compare our results with Love numbers fitted through dynamical modelling, we computed theoretical predictions using the

Table 1. Mean (ν) and standard deviation (σ) of the sample and line residuals (in pixels) for each satellite (*Cassini*-ISS data).

Observations	ν_{sample} (pix)	σ_{sample} (pix)	ν_{line} (pix)	σ_{line} (pix)	N	Satellite
ISS NAC (centroid fitting) prearrival	−0.2327	0.0000	0.8999	0.0000	1, 1	Titan
	−0.0404	0.2283	0.0866	0.1480	18, 18	Calypso
	0.0510	0.3000	0.0051	0.2042	21, 21	Telesto
	−0.0691	0.2381	0.0383	0.1657	11, 11	Helene
ISS NAC (MM centroid fitting) prearrival	−0.2527	0.1367	−0.1808	0.1945	11, 11	Atlas
ISS NAC (limb fitting)	0.0080	0.4883	0.1564	0.5422	155, 155	Mimas
	0.1015	0.6068	−0.0452	0.4768	1615, 1615	Enceladus
	−0.0764	0.3115	−0.0456	0.3164	452, 452	Tethys
	−0.0397	0.2794	0.0135	0.3003	752, 752	Dione
	−0.0916	0.3002	−0.0446	0.2608	649, 649	Rhea
	0.0696	1.7313	1.0702	1.4327	70, 70	Titan
	−0.0203	0.0969	0.8920	0.4051	3, 3	Hyperion
	−0.0511	0.6525	−0.0827	0.3566	80, 80	Iapetus
	0.0074	0.2576	−0.0725	0.2089	45, 45	Calypso
	−0.0656	0.2336	0.0220	0.1977	39, 39	Teltesto
	−0.0313	0.2527	−0.0375	0.2075	51, 51	Helene
	−0.0977	0.0770	0.0520	0.1059	3, 3	Pallene
ISS NAC (limb fitting) 3-d complex shape	0.0049	0.6912	0.1088	0.6991	166, 166	Atlas
	−0.0464	0.5251	−0.0664	0.5855	749, 749	Prometheus
	−0.0438	0.4417	−0.0693	0.5717	664, 664	Pandora
	−0.0349	0.3714	−0.1060	0.4758	532, 533	Epimetheus
	−0.0339	0.3552	−0.0692	0.4107	513, 513	Janus
ISS NAC (MM centroid fitting)	−0.0048	0.4345	−0.0722	0.3615	333, 333	Atlas
	−0.0110	0.1464	0.0067	0.1613	207, 207	Polydeuces
	0.0168	0.1752	−0.0215	0.2293	234, 234	Methone
	0.0005	0.1446	−0.0125	0.1316	169, 169	Anthe
ISS NAC green filter	−0.7505	1.0391	0.0077	0.7429	9, 9	Mimas
	0.3722	0.6972	0.2170	0.6830	49, 49	Tethys
ISS NAC red filter	−0.3327	0.0000	0.4694	0.0000	1, 1	Mimas
	0.2773	0.7195	0.5362	0.9669	11, 11	Tethys
ISS WAC (limb fitting)	−1.3335	0.0000	−0.0224	0.0000	1, 1	Mimas
	0.0863	0.0000	−0.7641	0.0000	1, 1	Dione
	0.2845	0.2258	0.2854	0.3724	2, 2	Rhea
	0.0372	0.0720	−0.2722	0.1168	4, 4	Calypso
	0.0749	0.1673	−0.1616	0.0895	6, 6	Telesto
	0.1602	0.1142	−0.2466	0.0567	2, 2	Helene
ISS NAC (limb fitting)	−0.0633	0.6675	−0.0027	0.3052	87, 87	Mimas
	0.0196	0.3406	0.1879	0.3616	36, 36	Tethys
ISS NAC green filter	−0.2658	0.6683	−0.1023	0.2637	19, 19	Mimas
	0.0382	0.3930	0.1385	0.3006	69, 69	Tethys
ISS NAC infra-red filter	−0.2092	0.8730	−0.0240	0.4375	19, 19	Mimas
	0.0177	0.3958	0.2544	0.5941	28, 28	Tethys
ISS NAC (limb fitting)	0.0359	0.9675	0.1487	0.5323	106, 106	Mimas
	−0.2353	0.3676	0.1374	0.3083	38, 38	Tethys
ISS NAC infra-red filter (limb fitting)	0.2662	0.4515	−0.4825	0.5388	4, 4	Mimas
	0.3280	0.7415	0.2231	0.5586	26, 26	Tethys

Notes. N is the number of observations by each satellite for each coordinate. Observations with residuals higher than 5 pixels were discarded. "MM centroid fitting" refers to the fitting technique presented in Zhang et al. (2021).

numerical approach described in Dewberry (2023). Briefly, this method amounts to a direct solution of Navier-Stokes, continuity, energy, and Poisson equations that have been linearized around an equilibrium, rotationally flattened model of Saturn and subjected to a tidal force with a harmonic time dependence.

We computed Love numbers as a function of tidal frequency for two rigidly rotating, dilute core models of Saturn (preliminary calculations suggested that differential rotation from Saturn's zonal winds has a marginal impact at the frequencies of interest): m23 is the best-fit model constrained by the ring seismological inference of Mankovich et al. (2023), and d21 is the model from Dewberry et al. (2021) with a dilute core extending over 72% of Saturn's equatorial radius. Both internal structure models were constructed using a combination of the MH13-SCvH (Militzer & Hubbard 2013; Miguel et al. 2016) and ANEOS (Thompson 1990) equations of state applied to

Table 2. Mean (ν) and standard deviation (σ) of the sample and line residuals (in pixels) for each satellite (*Cassini*-ISS data).

Observations	$\nu_{\rm sample}$ (pix)	$\sigma_{\rm sample}$ (pix)	$\nu_{\rm line}$ (pix)	$\sigma_{\rm line}$ (pix)	N	Satellite
ISS NAC (centroid fitting)	−0.0185	0.1947	−0.0499	0.2023	356, 356	Calypso
	−0.0329	0.1875	−0.0320	0.2573	360, 360	Telesto
	0.0112	0.2572	−0.1156	0.2695	322, 322	Helene
	−0.0091	0.2719	−0.0498	0.2394	279, 279	Pallene
ISS NAC red filter (limb fitting)	−0.9507	0.5119	0.0475	0.1209	4, 4	Mimas
	0.2170	0.5048	0.0704	0.2873	32, 32	Tethys
ISS NAC infra-red filter (limb fitting)	2.3577	0.1035	0.4656	0.3062	2, 2	Mimas
ISS NAC (limb fitting)	0.4281	0.1584	−0.1455	0.0494	2, 2	Dione
	1.1336	0.0000	0.1581	0.0000	1, 1	Iapetus

Notes. N is the number of observations per satellite for each coordinate. Observations with residuals higher than 5 pixels were discarded.

Table 3. Statistics of the ISS-NAC astrometric residuals computed in km.

Observations	$\nu_{\rm sample}$ (km)	$\sigma_{\rm sample}$ (km)	$\nu_{\rm line}$ (km)	$\sigma_{\rm line}$ (km)	N	Satellite
ISS NAC (limb fitting from free ellipse)	−1.3199	3.1132	−0.1538	2.7952	743, 743	Mimas
	−0.7422	3.2694	0.9055	3.0855	920, 920	Enceladus
	−0.4708	4.3961	0.7415	3.7807	922, 923	Tethys
	−0.1254	3.1857	0.3505	3.3475	1324, 1328	Dione
	−0.7188	3.0943	0.4697	2.8552	1345, 1347	Rhea
	−0.0777	12.6786	2.7285	10.1644	72, 88	Hyperion
	1.3099	5.3232	−1.1750	5.2649	1533, 1533	Iapetus

Notes. ν and σ respectively denote the mean and standard deviation of the residuals computed in RA and Dec. The N column shows the number of observations considered for the respective coordinate.

model mixtures of H, He, silicates, and ices. The theory of figures (Nettelmann et al. 2021) was used to compute the rotational flattening for these models of Saturn. In order to resolve peaks associated with resonant oscillation modes, which are formally infinite in the absence of dissipation, we included a purely constant kinematic viscosity, ν, and performed calculations for Ekman numbers $E_{\rm k} = \nu/(\Omega_{\rm S} R_{\rm S}^2) = 10^{-5}, 10^{-6}$.

For the tidal driving, we approximated satellite tidal potentials as point-mass potentials expanded in spherical harmonics up to degree $\ell = 12$ and computed k_{22} Love numbers as the real part of the ratio given in Eq. (5) (for $\ell = m = 2$). Including multiple harmonic degrees in the expansion of the tidal potential leads to some ambiguity in the definition of a response function defined for oblate bodies since one spherical harmonic of the tidal potential can drive another in the response (Dewberry & Lai 2022), but this effect is minimal for sectoral ($\ell = m$) harmonics.

Figure 1 compares the predicted k_{22} values to our measurements. Both models are compatible with the measured values within their uncertainties. The models predict a parabolic dependence of k_{22} on the tidal forcing frequency, with a minimum value near the forcing frequency of Mimas. This arises due to the Coriolis force on the tidal bulge, which is dominated by Saturn's fundamental modes (see Dewberry et al. 2021; Idini & Stevenson 2021). This dynamical tidal effect is necessary to explain Juno measurements of Jupiter's tidal bulge raised by Io (Lin 2023; Dewberry 2023; Dhouib et al. 2024) and should be present inside Saturn as well. Unfortunately, the substantial uncertainties of the measurements do not allow us to clearly detect this dynamical tidal effect. However, we note that the measured k_{22} is inconsistent with the value predicted by Wahl et al. (2017), who neglected dynamical tidal effects (i.e. they predicted the value of k_{22} at a tidal forcing frequency of zero). Similar to

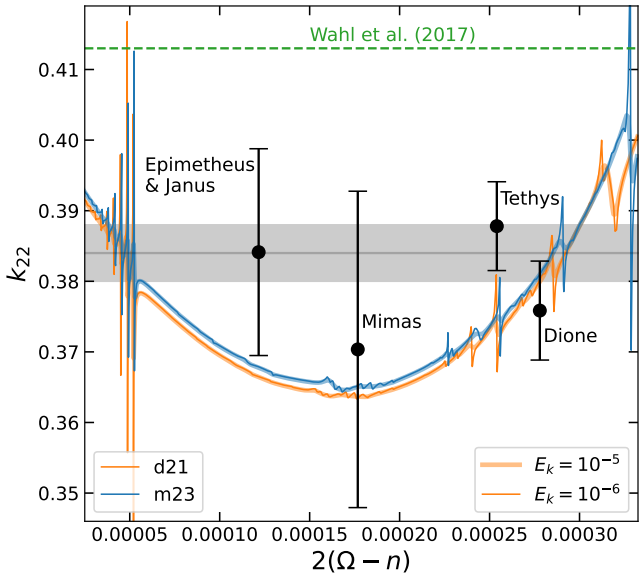

Fig. 1. Frequency variation in the Saturnian k_2 Love number from astrometric data. Black points are the measurements that allow for different k_2 values at each tidal forcing frequency, while the horizontal gray bar is the measurement found assuming a constant value of k_2. The orange and blue lines are the dynamical tidal response for two different Saturn models, with thick and thin lines corresponding to higher and lower viscosities, respectively. The dashed green line shows the hydrostatic $k_{22} = 0.4130$ computed by Wahl et al. (2017).

measurements for Jupiter, dynamical tidal effects likely explain the lower-than-expected value of k_{22} compared to predictions at a zero tidal forcing frequency.

In addition to the parabolic trend in k_{22}, the models also predict sharp, localized variations in this trend at certain tidal frequencies. They correspond to resonances with gravito-inertial modes of the planet, which enhance the tidal response and alter the value of k_{22} near the mode frequencies. These resonant frequencies are sensitive to the planetary model (in particular the stable stratification and rotation profiles), so a detection of resonant variations in k_{22} would provide strong constraints on the internal structure of Saturn. For instance, both models in Fig. 1 predict a sharp variation in k_{22} near the frequency of Tethys, which could account for its higher k_{22} value compared to the other moons if it is in a resonance lock with one of Saturn's gravito-inertial modes. The measurements are not yet precise enough to robustly detect these resonant effects, but measuring them in the future is an exciting prospect for constraining Saturn's internal structure and understanding whether resonance locking is occurring (Luan et al. 2018). Characterizing not just the real but also the imaginary parts of tidal Love numbers computed for realistic Saturn interior models would also help answer this question. Such a characterization introduces complications (Pontin et al. 2024) that are beyond the scope of this Letter, however, and we defer it to future investigations.

4. Conclusion

Using astrometric measurements of Saturn's moons, we were able to quantify Saturn's k_2 Love number at four different tidal frequencies. The measurement was facilitated by co-orbital moons, whose orbits are perturbed by the tidal bulge raised by the co-orbiting companion. Our Love number measurements are compatible with a constant value, within the error bars of the observations. They are also consistent with predictions from numerical models of the tidal response of Saturn, including contributions from fundamental modes, gravito-inertial modes, and inertial waves. Slightly more accurate future measurements will allow for the detection of dynamical tidal effects, including the possibility of resonantly excited gravito-inertial modes, which would allow us to place strong constraints on the internal structure of Saturn.

Acknowledgements. J.W. Dewberry is supported by the Natural Sciences and Engineering Research Council of Canada (NSERC), [funding reference # CITA 490888-16]. Q. Zhang was supported by the National Natural Science Foundation of China (No. 12373073, No. U2031104).

References

Acton, C. H. 1996, Planet. Space Sci., 44, 65
Cooper, N. J., Murray, C. D., Lainey, V., et al. 2014, A&A, 572, A43
Cooper, N. J., Lainey, V., Meunier, L. E., et al. 2018, A&A, 610, A2
Dewberry, J. W. 2023, MNRAS, 521, 5991
Dewberry, J. W., & Lai, D. 2022, ApJ, 925, 124
Dewberry, J. W., Mankovich, C. R., Fuller, J., Lai, D., & Xu, W. 2021, Planet. Sci. J., 2, 198
Dhouib, H., Baruteau, C., Mathis, S., et al. 2024, A&A, 682, A85
French, R. G., McGhee-French, C. A., Lonergan, K., et al. 2017, Icarus, 290, 14
Idini, B., & Stevenson, D. J. 2021, Planet. Sci. J., 2, 69
Iess, L., Militzer, B., Kaspi, Y., et al. 2019, Science, 364, aat2965
Lainey, V. 2016, Celest. Mech. Dyn. Astron., 126, 145
Lainey, V., Dehant, V., & Pätzold, M. 2007, A&A, 465, 1075
Lainey, V., Karatekin, Ö., Desmars, J., et al. 2012, ApJ, 752, 14
Lainey, V., Jacobson, R. A., Tajeddine, R., et al. 2017, Icarus, 281, 286
Lainey, V., Noyelles, B., Cooper, N., et al. 2019, Icarus, 326, 48
Lainey, V., Casajus, L. G., Fuller, J., et al. 2020, Nat. Astron., 4, 1053
Lainey, V., Rambaux, N., Cooper, N., Dahoumane, R., & Zhang, Q. 2023, A&A, 670, L25
Lainey, V., Rambaux, N., Tobie, G., et al. 2024, Nature, 626, 280
Lin, Y. 2023, A&A, 671, A37
Luan, J., Fuller, J., & Quataert, E. 2018, MNRAS, 473, 5002
Mankovich, C. R., Dewberry, J. W., & Fuller, J. 2023, Planet. Sci. J., 4, 59
Miguel, Y., Guillot, T., & Fayon, L. 2016, A&A, 596, A114
Militzer, B., & Hubbard, W. B. 2013, ApJ, 774, 148
Nettelmann, N., Movshovitz, N., Ni, D., et al. 2021, Planet. Sci. J., 2, 241
Newhall, X. X., Standish, E. M., & Williams, J. G. 1983, A&A, 125, 150
Pontin, C. M., Barker, A. J., & Hollerbach, R. 2024, ApJ, 960, 32
Porco, C. C., West, R. A., Squyres, S., et al. 2004, Space Sci. Rev., 115, 363
Tajeddine, R., Cooper, N. J., Lainey, V., Charnoz, S., & Murray, C. D. 2013, A&A, 551, A129
Tajeddine, R., Lainey, V., Cooper, N. J., & Murray, C. D. 2015, A&A, 575, A73
Thompson, S. L. 1990, ANEOS–Analytic Equations of State for Shock Physics Codes, Sandia Natl. Lab. Doc. SAND89-2951, http://prod.sandia.gov/techlib/access-control.cgi/1989/892951.pdf
Wahl, S. M., Hubbard, W. B., & Militzer, B. 2017, Icarus, 282, 183
Zhang, Q. F., Zhou, X. M., Tan, Y., et al. 2021, MNRAS, 505, 5253